Lithos 178 (2013) 186–196

Contents lists available at ScienceDirect

Lithos

journal homepage: www.elsevier.com/locate/lithos

Tschermak's substitution in antigorite and consequences for phase relations and water liberation in high-grade serpentinites

José Alberto Padrón-Navarta [a,b,*], Vicente López Sánchez-Vizcaíno [c], Joerg Hermann [b], James A.D. Connolly [e], Carlos J. Garrido [d], María Teresa Gómez-Pugnaire [d,f], Claudio Marchesi [d]

[a] Géosciences Montpellier, Univ. Montpellier 2 & CNRS, 34095 Montpellier, France
[b] Research School of Earth Sciences, The Australian National University, Canberra 0200, ACT, Australia
[c] Departamento de Geología (Unidad Asociada al IACT, CSIC-UGR), Escuela Politécnica Superior, Universidad de Jaén, Alfonso X El Sabio 28, 23700 Linares, Spain
[d] Instituto Andaluz de Ciencias de la Tierra (IACT), CSIC-UGR, Avenida de las Palmeras 4, 18100 Armilla, Granada, Spain
[e] Earth Sciences Department, Swiss Federal Institute of Technology, CH-8092 Zurich, Switzerland
[f] Departamento de Mineralogía y Petrología, Facultad de Ciencias, Universidad de Granada, 18002 Granada, Spain

ARTICLE INFO

Article history:
Received 14 November 2012
Accepted 4 February 2013
Available online 15 February 2013

Keywords:
Antigorite
Tschermak's exchange
Geothermobarometry
Serpentinite
Dehydration
Subduction zones

ABSTRACT

A model for the incorporation of alumina in FeO–MgO–Al_2O_3–SiO_2–H_2O (FMASH) serpentinites has been developed by considering ideal Tschermak ($Al_2Mg_{-1}Si_{-1}$) solid solution in antigorite. The antigorite model has been calibrated by fitting the experimental conditions for the decomposition of antigorite to chlorite + olivine + orthopyroxene + fluid in the FMASH system. The antigorite Al-contents predicted with this model are in agreement with natural observations and suggest a maximum alumina solubility in antigorite of 3.6 wt.% Al_2O_3 at 20 kbar–650 °C and of 4.5 wt.% Al_2O_3 at 3 kbar–560 °C. In the assemblage antigorite–olivine–chlorite–fluid, the Al-content of antigorite is buffered and temperature sensitive. This temperature sensitivity is the basis for a serpentinite geothermometer at greenschist, amphibolite and eclogite facies conditions. The buffered assemblage is stable in harzburgite compositions for relatively moderate amounts of Al_2O_3 (>1.8 wt.%) and is widespread in lherzolites, where it occurs together with diopside or, in a narrow temperature field, with tremolite.

1. Introduction

Serpentinites are the main carriers of water in the subducted slab and the dehydration reaction of antigorite is a fundamental process in the production of arc lavas (Schmidt and Poli, 1998; Ulmer and Trommsdorff, 1995). Serpentinites in the forearc mantle wedge act as a rheologically weak zone and play a role in decoupling the slab from the mantle (Angiboust et al., 2012; Hilairet and Reynard, 2009; Reynard, 2013). Furthermore, serpentinites are important for exhumation and preservation of high-pressure rocks (Agard et al., 2009; Gerya et al., 2002; Hermann et al., 2000; Malatesta et al., 2012). Current thermophysical models (e.g. Gerya et al., 2002; Hacker et al., 2003; van Keken et al., 2011) of subduction zones processes are based on a thermodynamic model of antigorite (Rüpke et al., 2004) that does not account for the solution of trivalent cations. In particular, trivalent aluminum is thought to have a significant influence on the stability of antigorite (Bromiley and Pawley, 2003; Ulmer and Trommsdorff, 1999). In antigorite, aluminum is believed to be incorporated through a coupled exchange where a Mg and a Si cations are substituted by two Al cations (i.e., Tschermak's exchange). The goal of this work is to develop a thermodynamic model for the Tschermak's exchange in antigorite and, thereby, improve the accuracy of subduction zone phase equilibrium modeling.

The MgO–SiO_2–H_2O (MSH) system is a good first order approximation for metamorphosed ultramafic rocks. The pressure and temperature stability of serpentine minerals has been investigated in this system and has been shown to be of importance for understanding their role in many geological processes (O'Hanley, 1996 and this special volume). Phase relations in the MSH system were established at low pressure by early experimentalists (cf. Bowen and Tuttle, 1949). However, it was recognized that the crystallographic structure and stability of MSH serpentine minerals is sensitive to minor amounts of exotic components. It is known that the substitution of trivalent cations in phyllosilicates such as lizardite (Caruso and Chernosky, 1979; Chernosky et al., 1988; Viti and Mellini, 1997) or phlogopite (Bucher-Nurminen, 1988) increases their stability field by reducing the misfit between the octahedral and tetrahedral sheets. A similar effect is expected for antigorite but its modular structure (i.e. reversal of the tetrahedral layer polarity), which thought to be dependent on composition, pressure, temperature and strain (Auzende et al., 2002, 2006; Mellini et al., 1987; Uehara and Shirozu, 1985; Wunder et al., 2001), makes this picture far more complex.

Fe–Mg partitioning between the ferromagnesian silicates in meta-ultramafic rocks produces that univariant reactions are transformed in divariant fields with a typical temperature interval of ca. 5–10 °C

* Corresponding author at: Research School of Earth Sciences, The Australian National University, Mills Road, Canberra 0200, Australia.
E-mail address: jose.padron@anu.edu.au (J.A. Padrón-Navarta).

0024-4937/$ – see front matter © 2013 Elsevier B.V. All rights reserved.
http://dx.doi.org/10.1016/j.lithos.2013.02.001

when the system is extended to FMSH composition. Apart from this limited effect, the incorporation of iron into the system is insufficient to create new topologies (O'Hanley, 1996; Trommsdorff and Evans, 1974; Ulmer and Trommsdorff, 1999; Worden et al., 1991). On the contrary, trivalent cations such as aluminum are strongly partitioned in chlorite and antigorite and therefore create new topologies in the MASH systems and produce a more prominent shift of the reactions (ca. 30–40 °C, Bromiley and Pawley, 2003).

Wunder and Schreyer (1997, their Fig. 7), Wunder (1998, his Fig. 6) and Ulmer and Trommsdorff (1995 their Fig. 1; 1999, their Figs. 6 and 9) made the most comprehensive studies of the phase relations in MSH system for ultramafic compositions at high pressure. Ulmer and Trommsdorff (1999) also discussed phase relations in the MASH system but these were limited to those involving only chlorite at temperature conditions higher than those for antigorite stability. Discrepancies in the thermal stability of the antigorite among these studies were attributed to differences in the amounts of various trivalent cations (mainly Al but also Cr) present in the antigorite natural starting material (Bromiley and Pawley, 2003). A full understanding of serpentinite phase relations in the MASH system and a quantitative knowledge of the effect of trivalent cation substitution in antigorite is necessary to improve the modeling of the conditions for dehydration reactions and mineral proportions in subduction zones.

It has been suggested that the Al-content in antigorite coexisting with chlorite and olivine is sensitive to temperature (Eggler and Ehmann, 2010; Li et al., 2004; Padrón-Navarta et al., 2008, 2011; Schwartz et al., 2013) and is thus a potential geothermometer for serpentinite. Geothermobarometry in serpentinite is traditionally hampered by the lack of assemblages buffering the antigorite composition, with the exception of the Fe–Mg exchange between antigorite and olivine (Evans et al., 2012). Therefore, serpentinite geothermobarometry customarily relies on the conditions at which breakdown reactions occur of phases like brucite, diopside or titanian clinohumite (which are, approximately, univariant and pressure independent) and/or alternatively on associated mafic assemblages (e.g. Scambelluri et al., 1995). Recently, Rebay et al. (2012) addressed how the pressure and temperature conditions of high-grade serpentinite could be constrained from mineral compositions in ultramafic assemblages. However, the proposed approach is based on Fe–Mg exchange between antigorite and other minerals and the Ca content in diopside, which are not very sensitive to changes in PT and hence are difficult to calibrate. The Al-content in antigorite may provide an independent constraint of the PT conditions for serpentinite phase equilibria. Such information would permit more precise estimation of the conditions for the subduction and exhumation structures recorded in serpentinite during orogenic cycles (Debret et al., 2013; Hermann et al., 2000; Rebay et al., 2012). Additionally, the relation between the Al-content and the modular structure in antigorite could be investigated more precisely without the need of indirect temperature constraints based on associated mafic rocks (cf. Auzende et al., 2006).

In this work, we compute Al isopleths in antigorite in different mineral assemblages as a function of pressure and temperature. This has been accomplished by considering a Tschermak's substitution in the extended ultramafic CFMASH system. The utility of this solid solution model is then discussed using serpentinite samples from the Betics (Cerro del Almirez, Spain) and the Western Alps (Zermatt-Saas), where metamorphic pressure–temperature conditions are well constrained. We will discuss the implications of the improved antigorite solution model for determining metamorphic conditions in serpentinites and for water liberation during subduction.

2. Tschermak's substitution in antigorite

2.1. Natural observations

Trivalent cations (Al, Cr and Fe^{3+}) are commonly present in antigorite (e.g. Uehara and Shirozu, 1985), aluminum being the most abundant by far (for a recent review of the ferric iron content in antigorite the reader is referred to Evans et al., 2012). Antigorite analyses were compiled to establish the mechanism of Al substitution (Fig. 1a). The analyses were normalized to 116 oxygens, corresponding to a polysome with $m = 17$; where m is the number of tetrahedra spanning a wavelength along the lattice parameter a. This definition of the formula unit results in the general formula $M_{3m\text{-}3}T_{2m}O_{5m}(OH)_{4m\text{-}6}$ (e.g. Mellini et al., 1987), where M and T represent the octahedral and tetrahedral sites respectively. For $m = 17$, which is considered the most representative polysome for antigorite in well crystallized serpentinites (e.g. Mellini et al., 1987), the antigorite formula for the MSH endmember is therefore $M_{48}T_{34}O_{85}(OH)_{62}$. The observed trends are compatible with a Tschermak's type substitution ($^{[6]}M^{2+} + ^{[4]}Si^{4+} = ^{[6]}Al^{3+} + ^{[4]}Al^{3+}$), where M^{2+} are divalent cations in the octahedral site (Mg, Fe, Mn and Ni, solid line in Fig. 1). Antigorite used in experimental studies (Fig. 1b) also plots on the tieline joining the antigorite MSH and MASH endmembers (atg and atgts respectively, white stars in Fig. 1, see below) with the exception of the antigorite used by Wunder and Schreyer (1997), most probably this anomaly is the effect of a large ferric iron content (1.09 wt.% Fe_2O_3). Therefore, in general, compositional data provide evidence that Al incorporation into antigorite can be described as a first approximation by the Tschermak's substitution.

2.2. Implications for the MASH compositional system

The addition of the Al_2O_3 component to the simple MSH system results in a pressure–temperature dependency of the Tschermak substitution in antigorite that modifies the MSH phase relations (Fig. 2a). The effect on the MSH phase relations can by illustrated by considering, for simplicity, Tschermak's exchange only in antigorite (Fig. 2). Talc, dense hydrous magnesium silicates (DHMSs) and humite series have been not included for simplicity. The qualitative phase relations in a Schreinemakers P–T projection (Fig. 2b) show the new invariant point possible in the four component MASH system that relates the six phases clinochlore, forsterite, enstatite, fluid, pyrope and antigorite (the latter spanning its composition from atg to atgts, Fig. 2a). The arrangement of the reactions and the location of this invariant point (ca. 60 kbar and 570 °C) were deduced experimentally by Bromiley and Pawley (2003) (their Fig. 2, although they did not consider the fluid absent reaction, [H_2O], our Fig. 2b).

In the MSH system, all phases are considered to have fixed stoichiometry so the only reactions are univariant (thin line in Fig. 2b). The introduction of Al into the system leads to the complication that phase compositions change as a function of pressure and temperature. Apart from clinochlore and pyrope (Fig. 2), the only phase that incorporates substantial amounts of Al (disregarding enstatite, but see Fockenberg and Schreyer, 1997) is antigorite. Al-content in antigorite changes continuously as a function of pressure, temperature and bulk composition (i.e. Al-isopleths, Fig. 2c) in the MASH system. To visualize these changes we arbitrary divide the antigorite solid solution into *pseudocompounds*, the conceptual basis for Gibbs free energy minimization in Perple_X (Connolly, 1990). In the case of antigorite, this involves a series of discrete compositions along the tieline joining the atg and atgts endmembers, that are labeled as low-Al antigorite and high-Al antigorite in a relative way. A practical consequence of the *pseudocompound* approach is that the continuous PT compositional changes in antigorite result in *pseudounivariant* reactions and *pseudoinvariant* points (dashed lines and black dots in Fig. 2c). For the definition of all these terms the reader is referred to Connolly (1990). The PT dependence of the Al-isopleths in antigorite is controlled by the buffering assemblage along the *pseudounivariant* reactions (e.g. [fo, en] is pressure dependent whereas [prp, en] is temperature dependent) (Fig. 2c). Of particular relevance for common serpentinite compositions is the *pseudounivariant* reaction [prp, en]:

$$\mathrm{Atg(low-Al) + clin = Atg(high-Al) + fo + H_2O.} \quad (1)$$

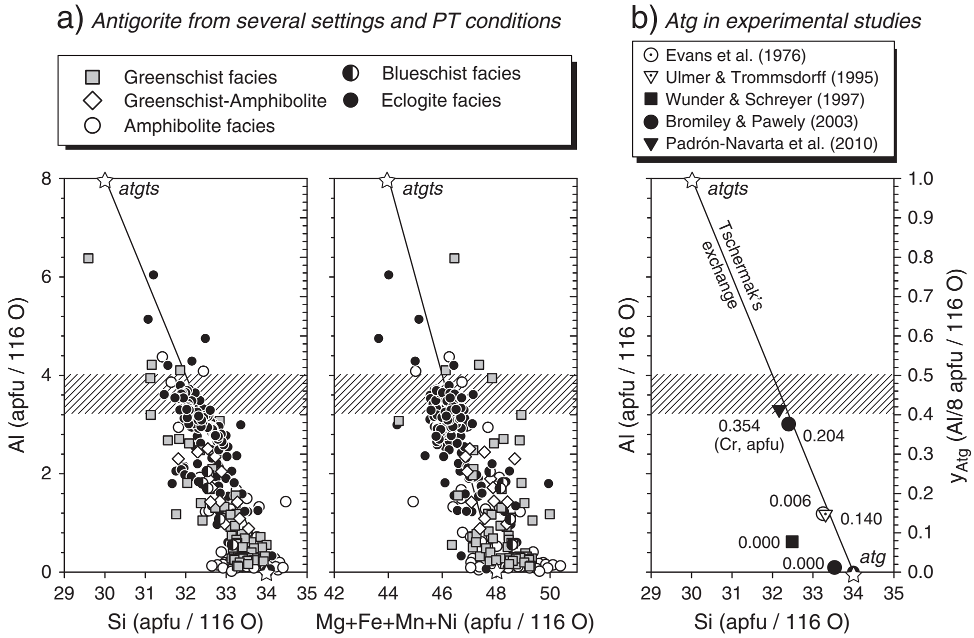

Fig. 1. (a) Compilation of antigorite microprobe analyses from the literature (461 analyses). The MSH and MASH antigorite endmembers are indicated with a star symbol joined by a Tschermak's exchange substitution (continuous line). The chosen structural formula for all analyses corresponds to a polysome $m=17$. Left axis in atoms per formula unit (apfu), right axis is the antigorite composition variable corresponding to the Tschermak's exchange ($y_{Atg}=Al/8$). Eclogite facies: Auzende et al. (2002, 2006), Facer et al. (2009), Khedr and Arai (2010, 2012), Khedr et al. (2010), Nozaka and Ito (2011), Nozaka (2005), Padrón-Navarta et al. (2008, 2011), Proenza et al. (2004), Rebay et al. (2012), Scambelluri et al. (1991), Smith (2010), Trommsdorff et al. (1998). Amphibolite facies: Auzende et al. (2002), Blais and Auvray (1990), Frost (1975), Khalil and Azer (2007), Li et al. (2004), Vance and Dungan (1977), Worden et al. (1991). Greenschist facies: Albino (1995), Azer and Khalil (2005), Dungan (1977), Evans et al. (1976), Li et al. (2004), O'Hanley and Wicks (1995), Peretti et al. (1992), Wicks and Plant (1979). Greenschist–amphibolite facies: Trommsdorff and Evans (1972). Blueschist facies: Uehara and Kamata (1994). (b) Compilation of antigorite composition used in experimental studies addressing its maximum stability field. Numbers indicate the Cr content in apfu. Gray horizontal band is the maximum solubility of Al in antigorite at 3–20 kbar obtained from the calculations.

The effect of this reaction on the divariant field between [prp] and [fo] univariant reactions is illustrated schematically through isobaric composition diagrams at different temperatures (Fig. 2c from 1 to 5). The sensitivity of this reaction to temperature makes it suitable for geothermometry. Its application to natural systems will be discussed after considering how to retrieve the thermodynamic properties of the Tschermak-antigorite endmember.

3. Calculation of the Tschermak-antigorite (atgts) endmember

Wicks and O'Hanley (1988) proposed that the maximum solubility of Al_2O_3 in antigorite from serpentinized lherzolites is ca. 4–5 wt.%. Higher Al_2O_3 concentrations (up to 6.1 wt.%) have been reported by Facer et al. (2009) in antigorite–chlorite intergrowths replacing spinel in xenoliths from the mantle wedge. It is unclear whether these latter compositions are real or due to a fine intergrowth between antigorite and chlorite. In any case, the election of the composition for the Tschermak-antigorite endmember (atgts), i.e., the extent of Tschermak's substitution, is of no relevance to the following discussion as long as (1) the Al-content of atgts is higher than the commonly observed content in antigorite from natural samples (Section 2.1) and (2) it does not plot at Al-rich compositions beyond the tieline joining clinochlore and orthopyroxene (Fig. 2a). In the latter case, the atgts endmember would be more stable than clinochlore at high temperature conditions, which is in disagreement with the topology proposed in Section 2.2 and with experimental (Bromiley and Pawley, 2003) and natural observations (Padrón-Navarta et al., 2011). Accordingly, the following composition $Mg^{M0}_{44}Al_4[Al_4Si_4]^{T1}Si^{T0}_{28}O_{85}(OH)_{62}$ (which corresponds to 8.98 wt.% Al_2O_3) has been chosen for the composition for the atgts endmember (Fig. 1).

Site occupancy must be considered in activity models for the assessment of the configurational entropy. It is believed that Al mixes equally in both octahedral and tetrahedral sites (e.g. Uehara and Shirozu, 1985) but because in antigorite all tetrahedral and octahedral sites are not equivalent the configuration entropy is a priori unknown. Because crystallographic constraints regarding the mixing are lacking, a conservative approach has been considered here, where Al and Si are assumed to mix on 8 tetrahedral sites (T1) coupled with the Mg and Al mixing in 4M1 sites. This mixing is independent of the mixing of other possible octahedral cations (i.e. $MgFe_{-1}$) in M1 and M0 sites. Based on these assumptions the ideal activity of atgts would be $a_{atgts}=256(z^{M0}_{Mg})^{44}(z^{M1}_{Al})^4(z^{T1}_{Al})^4(z^{T1}_{Si})^4$, where z^i_j is the molar site fraction of species j on site i.

The calibration of the atgts endmember was completed using the same approach as described by Tajčmanová et al. (2009) for titanium and ferric iron in biotite. First, the heat capacity and volumetric coefficients of atgts were computed by linear combination of other endmembers with known thermodynamic properties (taken from Holland and Powell, 1998 database, updated in 2002) and similar structure according to the reaction,

$$1\,atgts = 4\,clin + 9/17\,atg - 24/17\,br. \tag{2}$$

The entropy of the atgts endmember was raised by 8Rln (2) to account for the configurational entropy of Al and Si mixing in T1. Lastly, the Gibbs free energy of formation of the atgts endmember was adjusted to fit observed natural and experimental mineral compositions at known PT conditions of equilibration. For this purpose, the following reaction has been used for the calibration

$$1\,atgts = 4\,clin + 6\,fo + 6\,en + 15\,H_2O. \tag{3}$$

Several authors have experimentally investigated this reaction but only Bromiley and Pawley (2003 and personal communication, 2012) and Padrón-Navarta et al. (2010) have provided enough chemical

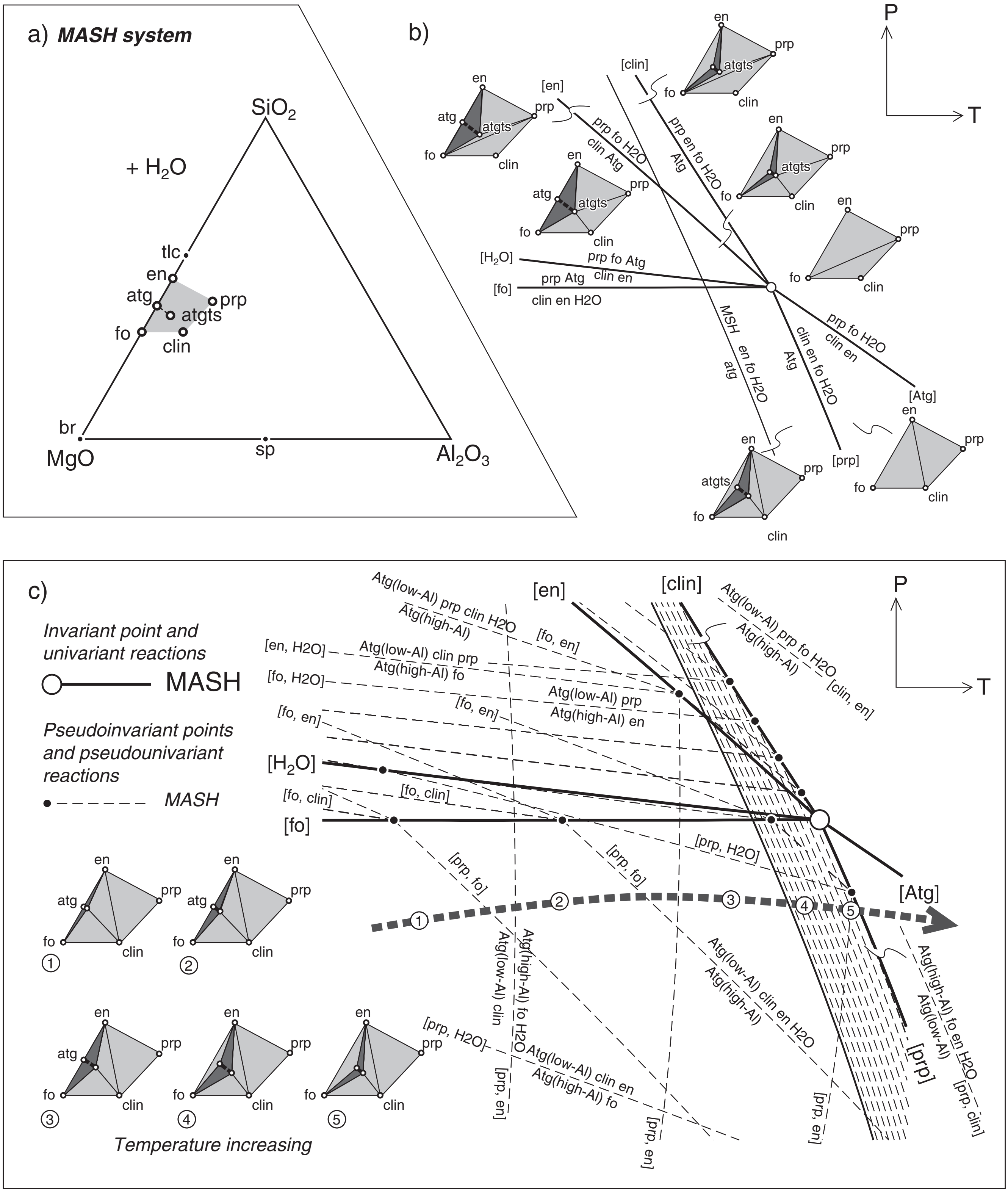

Fig. 2. (a) Compositional diagram in the $MgO–Al_2O_3–SiO_2–H_2O$ system projected through H_2O with the phases considered in this work. Mineral abbreviations are after Whitney and Evans (2010). The extent of solid solution through Tschermak's type substitution in antigorite is indicated with dashed lines. (b) Schreinemaker's projection for a part of the MASH system considering only antigorite as a solid solution. Absent phase for each reaction is indicated in brackets. (c) Schematic arrangement of pseudoinvariant points and pseudounivariant reactions emanating from (b). An illustration of the antigorite compositional change with temperature along one PT path (thick dashed line) is given from 1 to 5. Two-phase assemblages are trivariant (black), three-phase assemblages are divariant (gray). Compatibility diagrams computed with CSpace (Torres-Roldán et al., 2000).

data of the phases, which are necessary for the recalibration of the atgts endmember. Because the experiments were done in the FMASH system, it is necessary to compute the activity of the MASH endmembers by using activity-composition expressions that in turn depend on the solid solution model chosen for the ferromagnesian phases (Table 1).

Table 1
Solid solution model used in this work. Chemical formula are expressed in terms of the composition al variables x and y that may vary between zero and unity. Thermodynamic data for the iron endmembers antigorite and brucite are from Rüpke et al. (2004).

Symbol	Phase	Formula	Solution model type	Source
Atg	Antigorite	$Mg_{x(48-y)}Fe_{(1-x)(48-y)}Al_{8y}Si_{34-y}O_{85}(OH)_{62}$	Reciprocal (ideal)	This work
Chl	Chlorite	$Mg_{x(6-y)}Fe_{(1-x)(6-y)}Al_{2y}Si_{4-y}O_{10}(OH)_8$	Reciprocal (regular)	Modified[1] from Holland et al. (1998)
Ol	Olivine	$Mg_{2x}Fe_{2(1-x)}SiO_4$	Regular	Evans et al. (2012)
Opx	Orthopyroxene	$Mg_{x(2-y)}Fe_{(1-x)(2-y)}Al_{2y}Si_{2-y}O_6$	Reciprocal with speciation (regular)	Holland and Powell (1996)
Tlc	Talc	$Mg_{x(3-y)}Fe_{(1-x)(3-y)}Al_{2y}Si_{4-y}O_{10}(OH)_8$	Reciprocal (ideal)	Holland and Powell (1998)
Br	Brucite	$Mg_{2x}Fe_{2(1-x)}(OH)_2$	Ideal	–
Cpx	Clinopyroxene	$Ca_yMg_{xy}Fe_{(1-x)y}Al_ySi_2O_6$	Speciation (regular)	Holland and Powell (1996)
Tr	Clinoamphibole	$Ca_2Mg_{(3+2y)x}Fe_{(3+2y)(1-x)}Al_{3-3y}Si_{7+y}O_{22}(OH)_2$	Reciprocal (regular)	Wei and Powell (2003); White et al. (2003)
Grt	Garnet	$Mg_{3x}Fe_{3y}Ca_{3(1-x-y)}Si_3O_{12}$	Regular	Holland and Powell (1998)

[1] The amesite endmember was excluded.

The enthalpic correction (δH_{atgts}) for the atgs endmember necessary to bring the free energy change of reaction (3) to zero based on the observed mineral compositions (Table 2) is scatter around zero, suggesting that correction for the enthalpy of the atgts endmember estimated from reaction (2) is insignificant. The reduced number of experimental pairs does not allow a statistical analysis of the dependence of this parameter from pressure and temperature although it seems that the correction for the high-pressure pairs (>29 kbar) differs from the lower pressure ones (Fig. 3). This could be an effect of an inappropriate equation of state (EoS) for antigorite at high pressure. The new EoS for Al-bearing antigorite proposed by Hilairet et al. (2006a,b) and Nestola et al. (2010) produces a pronounced shift of reaction (3) to lower temperature at high pressure, which is in disagreement with the experimental observations in the FMASH system by Bromiley and Pawley (2003) therefore increasing the scattering of the correction parameter (Fig. 3). Hence in the current calculations we used the EoS from the Holland and Powell (1998, revised 2002) database.

4. Results

In order to depict the quantitative influence of the Tschermak's substitution in antigorite on phase relations, phase diagram sections were computed with Perple_X 6.6.7 (Connolly, 2009) as function of pressure and temperature (Fig. 4) and as a function of temperature and Al_2O_3-content (Fig. 5) using the thermodynamic database of Holland and Powell (1998, updated in 2002) and solid solution models specified in Table 1.

4.1. Serpentinite derived from harzburgite (Cerro del Almirez, Betic Cordillera): FMASH system

To test the antigorite solution model, a phase diagram section was computed as a function of pressure and temperature (Fig. 4) for the bulk composition of a common high-grade serpentinite (olivine and antigorite bearing) from the Cerro del Almirez ultramafic massif (sample Al06-44, Padrón-Navarta et al., 2011, Table 3). The ferrous iron content of this sample was obtained by potentiometric analyses using permanganate as oxidation agent. Ferric iron was calculated from the difference of the total iron measured by XRF and the measured ferrous iron. The resulting ferric iron corresponds very well with the observed modal amount of magnetite in this sample (5 wt.%). Therefore an Fe_2O_3 amount of 3.37 wt.% corresponding to the magnetite proportion of this sample was subtracted from the bulk rock. This implies an amount of 0.90 wt.% Fe_2O_3 in antigorite for this sample; a value that is in the range (0.16–1.94 wt.% Fe_2O_3 with an average value of 0.83 wt.%) of ferric iron in antigorite recently proposed by Evans et al. (2012). In our computed section (Fig. 4), antigorite coexists either

Table 2
Mineral composition and PT conditions of the brackets for reaction (3) used to retrieve the enthalpic correction for the atgts endmember (δH_{atgts}). P_1T_1 and P_2T_2 are the low and high PT conditions of the brackets. The compositional variable x for Atg, Opx, Ol and Chl is the Mg/(Fe + Mg) ratio whereas y_{Atg} = Al/8, y_{Opx} = Al/2 and y_{Chl} = Al/2 in apfu.

Pair	P_1 (kbar)	T_1 (°C)	Run no.	x_{Atg}	y_{Atg}	(1σ)	P_2 (kbar)	T_2 (°C)	Run no.	x_{Ol}	x_{Opx}	y_{Opx}	(1σ)	x_{Chl}	y_{Chl}	(1σ)	Source
1	20.0	650	AFEC5	0.92	0.38	0.02	20.0	700	AFEC4	0.91	0.94	0.16	0.06	0.93	0.86	0.18	[1]
2	29.0	660	AFEC2	0.92	0.38	0.02	29.0	680	AFEC3	0.91	0.94	0.16	0.06	0.93	0.86	0.18	[1]
3	50.0	600	AFEC6	0.92	0.38	0.02	45.0	670	AFEC8	0.91	0.94	0.16	0.06	0.93	0.86	0.18	[1]
4	50.0	600	AFEC6	0.92	0.38	0.02	55.0	600	SATG3	0.91	0.95	0.01	0.02	0.93	0.86	0.18	[1]
5	16.0	660	C2989	0.94	0.38	0.09	16.0	680	C3004	0.89	0.88	0.01	0.01	0.95	0.73	0.08	[2]
6	18.0	680	C3044	0.94	0.45	0.09	18.0	700	C3012	0.89	0.89	0.01	0.01	0.94	0.76	0.07	[2]
7	20.0	670	C3003	0.93	0.40	0.06	20.0	700	C3011	0.89	0.91	0.02	0.01	0.95	0.78	0.04	[2]
8	22.5	665	C3220	0.94	0.40	0.04	22.5	680	D756	0.89	0.90	0.02	0.01	0.94	0.81	0.02	[2]
9	22.5	665	C3220	0.94	0.40	0.04	25.0	670	C2967	0.89	0.90	0.04	0.01	0.94	0.80	0.04	[2]

Pair	P (kbar)	T (°C)	*a* (atgts)	*a* (en)	*a* (clin)	*a* (fo)	δHatgts (kJ)
5	16.0	680	0.165	0.778	0.193	0.813	−11.5
6	18.0	690	0.276	0.794	0.225	0.813	−5.0
1	20.0	675	0.066	0.755	0.380	0.849	−11.0
7	20.0	685	0.194	0.820	0.271	0.813	−1.7
8	22.5	673	0.194	0.804	0.308	0.813	−4.9
9	25.0	668	0.194	0.790	0.291	0.813	−10.3
2	29.0	670	0.066	0.756	0.380	0.849	10.3
3	47.5	635	0.066	0.756	0.384	0.850	13.0
4	52.5	600	0.066	0.897	0.388	0.844	8.2
							−1.4

[1] Bromiley and Pawley (2003). [2] Padrón-Navarta et al. (2010).
1σ values for x variable are typically 0.01–0.02.
Data shown in bold indicates the average value.

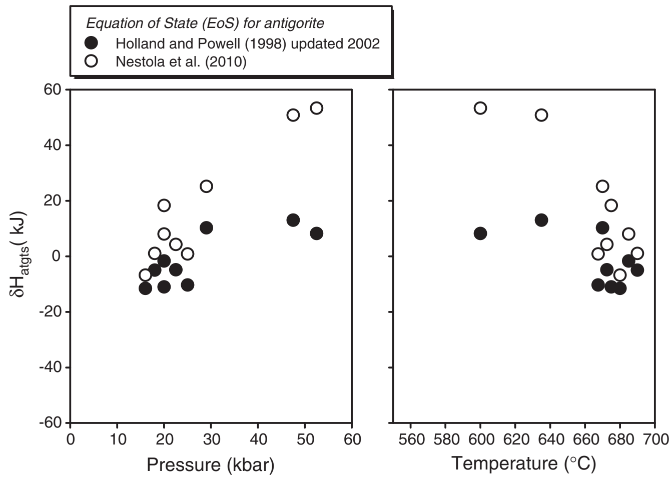

Fig. 3. Values of δH_{atgts} retrieved from calibration of reaction (2) (Table 2) vs. pressure and temperature. Note the dispersion and the correlation with pressure and temperature of the δH_{atgts} values when the antigorite EoS from Nestola et al. (2010) is used (empty symbols).

with Chl or Ol (in fields with variance 4, dark fields) or with Chl and Ol (variance 3, light fields). The Al-content in antigorite is only buffered in the low variance assemblage, for which it ranges from $y_{Atg} = 0.30–0.35$ (where $y_{Atg} = Al/8$ in apfu, 116 O, dashed lines in Fig. 4). The maximum antigorite thermal stability for this sample is 670 °C located at ca. 20 kbar.

Pressure and temperature conditions from the Cerro del Almirez serpentinite are well constrained (ca. 630 °C and 18 kbar, white field in Fig. 4, Padrón-Navarta et al., 2011 and reference therein). The stable mineral assemblage (Atg–Ol without chlorite) and the composition of antigorite and olivine computed at these PT conditions are in excellent agreement with the natural observations (Table 3).

4.2. Effect of spinel proportion in the phase relations for harzburgite: T–X sections

The aluminum content in serpentinite derived from harzburgites is related to the original proportion of spinel and, to a lesser extent, to the Al-content in the orthopyroxene. Low bulk Al-content in the protolith will eventually control the Al-content in antigorite in not buffered assemblages. At higher proportion of spinel in the protolith, antigorite will coexist with chlorite and its Al-content will depend mainly on temperature as a consequence of reaction (1) (cf. Fig. 2c). Li et al. (2004) reported a set of low-Ca serpentinites (<0.02 wt.% CaO) from Zermatt-Saas ophiolite with contrasting normative proportion of spinel, which are suitable to illustrate the effect of bulk Al_2O_3 content in the composition of antigorite and its phase relations during metamorphism. To quantify these relations we computed an isobaric phase diagram section as a function of temperature and bulk Al_2O_3-content at water-saturated conditions (Fig. 5 at 20 kbar), where X represents the proportion between two bulk compositions (X1 and X2) and is related to the amount of alumina. In the present example, X1 is an Al-free equivalent of their sample lg13 (i.e. projected into the FMSH system) and X2 corresponds to sample lg33 (Table 3). These compositions were selected to represent a spinel-free harzburgite and a harzburgite with a 2.7 wt.% of normative spinel (Li et al., 2004). Al-isopleths in antigorite (y_{Al} continuous lines) and orthopyroxene (y_{Opx} dashed lines) are shown in Fig. 5.

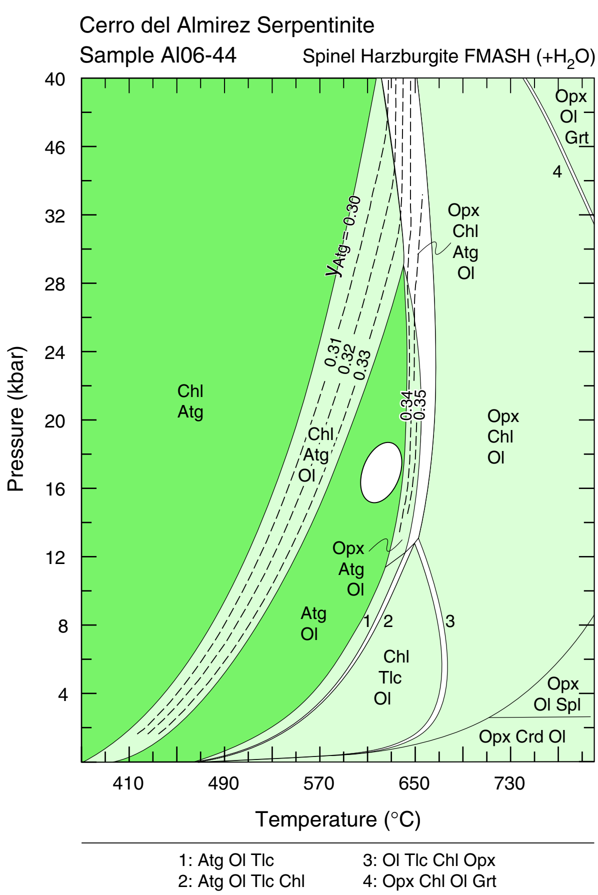

Fig. 4. Fluid saturated PT pseudosection for a common serpentinite bulk composition from Cerro del Almirez (Betic Cordillera, Spain) in the FMASH system (sample Al06-44, Table 3). Contours of the Al-content in antigorite (y_{Atg}) are shown. The white ellipse indicates stability PT conditions for this sample (cf. Table 3). White, light colored and dark colored fields represent stability variances of two, three and four, respectively.

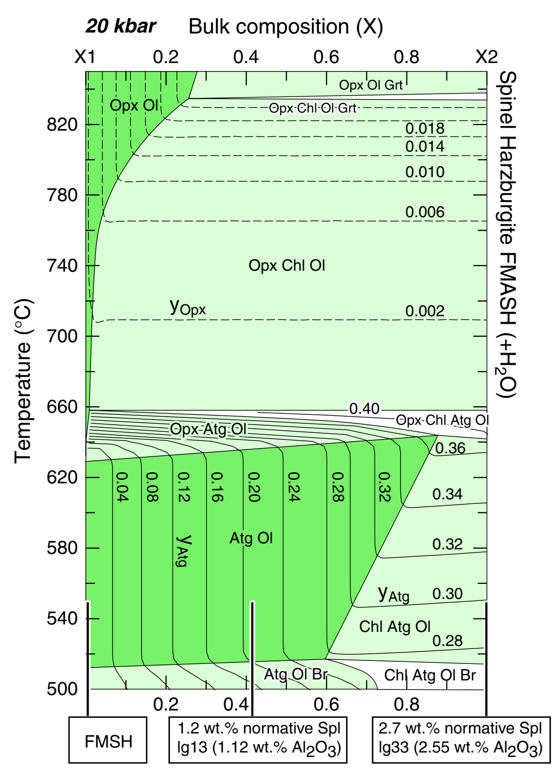

Fig. 5. Isobaric T–X pseudosection at 20 kbar where X1 is the projection of sample lg13 into the FMSH system and X2 corresponds to sample lg33 (Table 3). Al-isopleths for antigorite (continuous lines) and orthopyroxene (dashed lines) are shown.

Table 3
Bulk rock (BR) composition used in the modeling (cf. Figs. 4–6). Also shown are the mineral compositions of the two selected examples discussed in the text (Figs. 4 and 6).

Locality	Cerro del Almirez (Betic Cordillera)[1]						Zermatt-Sass (Western Alps)[2]			
	Al06-44 (Fig. 4)						lg13 (Fig. 5)	lg33 (Fig. 5)	lr21 (Fig. 6)	
wt.%	BR	Mag[3]	Atg		Ol		BR	BR	BR	Atg
			n = 7	1σ	n = 8	1σ				n = 10
SiO_2	40.34	<0.03	41.60	(0.22)	40.67	(0.06)	40.30	39.97	41.37	41.74
TiO_2	0.10	0.13	0.02	(0.01)	0.01	(0.01)	0.03	0.02	0.11	0.01
Cr_2O_3	0.43	2.10	0.44	(0.03)	0.01	(0.01)	0.44	0.35	0.60	0.6
Al_2O_3	2.81	0.03	3.03	(0.13)	0.00	(0.00)	1.12	2.55	4.06	3.03
Fe_2O_3	4.26	67.3	–	–	–	–	–	–	–	–
FeO	2.87[m]	29.0	3.98	(0.05)	11.03	(0.11)	5.78	5.24	6.32	4.84
MnO	0.09	0.28	0.08	(0.06)	0.33	(0.04)	0.11	0.09	0.10	0.1
MgO	37.48	1.14	36.72	(0.30)	47.80	(0.08)	42.67	39.10	35.03	37.63
CaO	0.07	<0.02	0.00	(0.01)	0.01	(0.01)	0.02	0.01	2.93	0.06
Na_2O	0.04	<0.03	0.00	(0.00)			–	–	–	–
LOI	11.47		11.81[c]	(0.08)			8.79	12.00	8.95	
Total	99.5				100.1		99.53	99.57	99.69	88.17
		x_{Atg}	0.943	(0.001)					x_{Atg}	0.933
		y_{Atg}	0.348	(0.023)					y_{Atg}	0.345
				x_{Ol}	0.885	(0.001)				

Bulk composition in the FMAS(H) system of sample Al06-44 after subtracting 5 wt.% of magnetite and in the CFMAS(H) system of sample lr21 used in the pseudosections. Also shown are the computed composition of Atg and Ol at 630 °C and 18 kbar for sample Al06-44 and 625 °C (Fig. 4) and 22.5 kbar for sample lr21 (Fig. 6).

wt.%	BR		Atg		Ol		BR	BR	BR	Atg
SiO_2	40.34		42.78		40.46		40.30	39.97	41.37	42.61
Al_2O_3	2.81		2.99		–		1.12	2.55	4.06	2.95
FeO	3.75		2.41		12.01		5.78	5.24	6.32	3.39
MgO	37.42		39.65		47.54		42.67	39.10	35.03	38.93
CaO	–		–		–		–	–	2.93	–
		x_{Atg}	0.957						x_{Atg}	0.953
		y_{Atg}	0.336						y_{Atg}	0.334
				x_{Ol}	0.876					

[1] Data are from Padrón-Navarta et al. (2011).
[2] Data are from Li et al. (2004).
[3] Data are from Trommsdorff et al. (1998), sample Al95-20.
[c] calculated.
[m] measured.

At bulk compositions with low Al-contents (X<0.6–0.85), antigorite coexists with brucite and olivine at T<510 °C and with olivine between 510 and 630 °C, whereas at higher X, it coexists additionally with chlorite. In the latter case, y_{Atg} is strongly dependent on temperature increasing from 0.25 to 0.36 in a temperature range from 520 to 620 °C.

For X<0.85, the decomposition of antigorite at 20 kbar initiates in the trivariant field Opx–Atg–Ol and continues through the divariant field Opx–Chl–Atg–Ol (white field in Fig. 5). In these assemblages, y_{Atg} increases to 0.40 at 660 °C. The temperature interval of the trivariant field Opx–Atg–Ol reduces with increasing the bulk Al_2O_3 contents and ranges from 30 °C at X = 0.01 to zero at X = 0.85. In contrast, the temperature extent of the divariant field Opx–Chl–Atg–Ol expands with increasing the bulk Al_2O_3 contents and reaches ca. 20 °C at X2 for a 2.7 wt.% normative spinel. At 20 kbar, the Tschermak's content in orthopyroxene produced by the antigorite breakdown is temperature dependent but its extent is limited (ranging from y_{Opx} = 0.002 to 0.026 in the Opx–Chl–Ol field, Fig. 5).

4.3. Serpentinite derived from lherzolite (Zermatt-Saas, Western Alps): CFMASH system

For a typical lherzolite (from Li et al., 2004; sample lr21), the introduction of Ca results in the occurrence of diopside and tremolite (Fig. 6). Tremolite is stable in a narrow temperature interval (Fields 2 and 3 in Fig. 6) close to the antigorite decomposition conditions at T = 650 °C and P<18–20 kbar (López Sánchez-Vizcaíno et al., 2005; Rebay et al., 2012; Trommsdorff and Connolly, 1996; Yang and Powell, 2008).

Aluminum content in serpentinites derived from fertile compositions and pyroxenites are generally high (>3–4 wt.% Al_2O_3) because, in addition to spinel, clinopyroxene also hosts Tschermak's content (e.g. Müntener and Hermann, 1994). The modeled sample lr21 contains 4.06 wt.% Al_2O_3 and, as a result, all fields in Fig. 6 containing antigorite coexist with chlorite, resulting in trivariant and divariant assemblages. The Al-content in antigorite is therefore buffered in a wider PT range compared to harzburgite (compare isopleths for y_{atg} in Figs. 4 and 6). Al-content increases from low values of y_{atg} (0.18–0.20) below 490 °C at ultra-high pressure conditions (25–40 kbar) to high values of y_{atg} (up 0.5) at 570 °C and 3 kbar when coexisting with tremolite at amphibolite facies conditions.

Based on associated mafic rocks, Li et al. (2004) inferred that the PT path followed by the Zermatt-Saas ophiolites (thick line in Fig. 6) could also be recognized in chemically distinct generations of olivine and antigorite. A similar conclusion was recently reached by Rebay et al. (2012) but based on Fe–Mg exchange and Ca-content in the newly formed diopside. The extension of the antigorite solid solution to the FMASH system gives us the opportunity to investigate these changes in a more quantitative way. Several metamorphic stages were recognized by Li et al. (2004). Three of these stages are superimposed on the PT path shown in Fig. 6, where B represents the peak metamorphic conditions and C and D are related to exhumation. The computed y_{atg} values at the peak conditions (Table 3) are in excellent agreement with those reported for the same sample (y_{atg} = 0.334 vs. 0.345 or 2.95 vs. 3.03 wt.% in Al_2O_3, respectively). A direct comparison of the antigorite composition for the retrograde path is not possible using exclusively sample lr21 because it only records the stage B. In any case, the

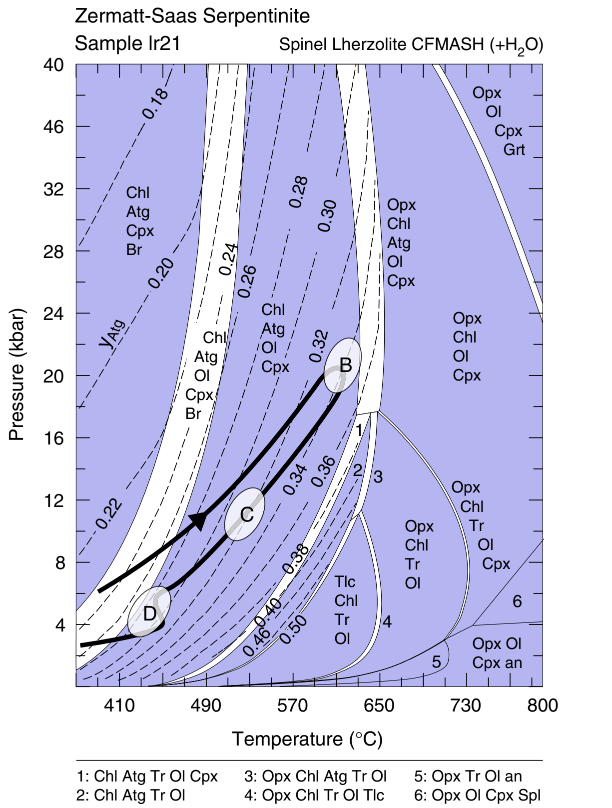

Fig. 6. Fluid saturated PT pseudosection for a Ca-bearing serpentinite bulk composition from Zermatt-Saas (Western Alps, Italy) in the CFMASH system (sample lr21, Table 3). Contours of the Al-content in antigorite (y_{Atg}) are shown. Part of the PT path deducted by Li et al. (2004) is indicated with a thick line. B stage corresponds to peak metamorphic conditions for this sample (see Table 3 for the mineral composition computed at these conditions).

antigorite computed composition along the PT path for this sample qualitatively shows a similar trend ($y_{atg}=0.36$–0.22, $x_{atg}=0.95$–0.97 from B to D) to the one observed in Zermatt-Saas ($y_{atg}=0.39$–0.17, $x_{atg}=0.92$–0.97 from B to D).

5. Discussion

5.1. Assessment of the antigorite solid solution in the MASH system

A comparison of the phase equilibrium calculations (Figs. 4–6) for high-grade serpentinites suggests that the proposed solution model correctly reproduces the observed Al-contents in natural antigorite. The maximum Al-solubility in antigorite is in the order of 4.0 apfu at 3 kbar and 3.2 apfu at 20 kbar (4.5 and 3.6 wt.% Al_2O_3, respectively). These values are in reasonable agreement with, although slightly lower than, the maximum value (ca. 4–5 wt.%) observed by Wicks and O'Hanley (1988) in natural antigorites from a serpentinite derived from a lherzolitic composition (see also Fig. 2a). Most likely, the higher Al-content observed in nature reflects the effect of chromium and ferric Tschermak's substitution in antigorite, which is not accounted for in the model. Al-content in orthopyroxene produced by the antigorite dehydration is predicted to be very low (<0.01 apfu) in excellent agreement with natural observations (0–0.01 apfu, Padrón-Navarta et al., 2011; Trommsdorff et al., 1998) and experiments (0–0.04 apfu, Padrón-Navarta et al., 2010).

In this paper, it has been assumed that the antigorite composition corresponds to a fixed polysome. It is also implicit that the Tschermak's substitution applies only to this latter formula. These two assumptions are a simplification because: (1) variations in the polysome at the crystal scale are often observed in nature (e.g. $m=13$–21, Mellini et al., 1987); and (2) it is expected that the variation with P and T in both the polysome and the Al-content are not independent (Bromiley and Pawley, 2003; Padrón-Navarta et al., 2008, 2011; Uehara and Shirozu, 1985; Wunder et al., 2001). Moreover, the effect of kinetics and deformation has been also suggested as a limiting factor controlling the antigorite structure (Auzende et al., 2002, 2006). Deprotonation due to imbalanced trivalent cations (c.f. Fuchs et al., 1998) may further complicate this picture. Nevertheless, the overall good agreement we obtain from our calculations with studies from natural rocks indicates that our assumptions provide a good approximation.

Chlorite compositions from natural serpentinite (from both harzburgitic and lherzolitic protoliths) are less aluminous (i.e. pennine, with typically 12.0–13.5 wt.% Al_2O_3, Müntener and Hermann, 1994; Rebay et al., 2012; Trommsdorff et al., 1998) than clinochlore endmember (17.13 wt.%). Indeed, clinochlore composition only occurs in antigorite-free metaclinopyroxenites (Müntener and Hermann, 1994). Computed chlorite composition coexisting with antigorite is, however, invariably close to clinochlore (ca. 1.98–2.00 apfu Al). Although this fact has no implications for the antigorite solution model or the applicability of reaction (1), it has the consequence that our computed modal proportion of chlorite is slightly underestimated.

5.2. A potential geothermobarometer for antigorite serpentinite

Mafic rocks display a variety of parageneses with changing metamorphic grades, and thus have been used to define different metamorphic facies. In contrast, ultramafic rocks have large stability fields for single assemblages (e.g. Fig. 4). While such a situation is advantageous for record of overprinting structures in serpentinites (Debret et al., 2013; Hermann et al., 2000; Rebay et al., 2012), it complicates the determination of associated metamorphic conditions. In this contribution, we have shown that the Al content of antigorite in buffered assemblages provides the opportunity for constraining metamorphic conditions in antigorite serpentinites. The isopleths of Al in antigorite within the investigated P–T range display a positive slope with an increased curvature at pressures below 10 kbar (Figs. 4 and 6). Hence, for eclogite facies serpentinites, the Al content in antigorite is primary a function of temperature. On the other hand, for greenschist and amphibolite facies serpentinites, the Al content in antigorite can serve to constrain pressures, if an independent temperature constrain is available.

The Al-isopleths for antigorite are not aligned with facies boundaries deduced from mafic rocks. Indeed, our tentative classification based on metamorphic facies does not reveal a clear pattern (Fig. 1a). Al-content in antigorite from all facies ranges from nearly zero to ca. 4 apfu (based on 116 oxygens, $m=17$). Antigorite from eclogite facies conditions clusters at about 3 apfu but still displays a significant spread. It is important to note that in the compilation of natural antigorite data, further factors can lead to some deviations. First at all, not all the plotted antigorites were in equilibrium with a buffering aluminum phase. Moreover, the scattering of the data around the exchange vector is likely caused by the modular structure of the antigorite (i.e. polysomatism) resulting in a non-fixed chemical formula. Minor changes in the ratio between tetrahedral and octahedral sites are expected to occur at different metamorphic grades (e.g. Mellini et al., 1987; Wunder et al., 2001) thus causing the deviation from the ideal exchange vector (here assumed to occur for a fixed polysome, $m=17$). Cr and Fe^{3+} could also play a role in the scattering (Evans et al., 2012). Moreover, the phyllosilicate nature of antigorite is prone to produce mixing analysis due to fine intergrowths between antigorite–chlorite (most probably the ones with Al>4.0–4.5 apfu in Fig. 1a) and/or antigorite–lizardite–chrysotile.

Our calculations show that modest amounts of Al_2O_3 in harzburgitic compositions are required for the coexistence of antigorite with chlorite and olivine or brucite (Fig. 5). Moreover, the common occurrence of metaclinopyroxene and more lherzolitic compositions with higher Al_2O_3 contents (Fig. 6) expands the fields at which fully buffered assemblages are stable, thus allowing a wider application of the Al-in antigorite geothermometer. Therefore, by choosing appropriate bulk rock compositions, it is possible to use the Al content of antigorite over a wide range of conditions to constrain metamorphic conditions in serpentinites.

Padrón-Navarta et al. (2011) observed a significant decrease in Al-content (from 3.4 to 1.53 apfu) in antigorite associated with chlorite in the transitional lithologies occurring between Atg–serpentinite and prograde Chl–harzburgite from the Cerro del Almirez ultramafic massif. They interpreted the decrease in Al as a prograde feature due to the growth of chlorite. The solution model for antigorite presented here, however, predicts that (1) the antigorite Al-content should increase with temperature, (2) the breakdown of the Al-bearing antigorite at the PT of interest should result in a trivariant field containing Opx–Atg–Ol, and (3) chlorite will coexist with the previous assemblage at slight higher temperatures (ca. 20 °C, Fig. 4). One explanation for this apparent inconsistency would be that this transition zone has been modified during exhumation. Thus the relatively low Al content of antigorite in this zone records the retrograde path and re-equilibration during cooling rather than peak metamorphic conditions. This example highlights how the new information of Al in antigorite helps to clarify formation conditions of serpentinites.

Other trivalent cations such as Cr and Fe^{3+} are very likely to be incorporated in antigorite also through a Tschermak's like substitution (Evans et al., 2012). Thus, ideally they should be considered for modeling in an independent way. Unfortunately, it is unfeasible to isolate their contributions, as our anchors for the regression are natural antigorite containing a finite amount of Cr and Fe^{3+}. Because in our calibration we use natural antigorites, the estimated enthalpic correction already includes the effect of these other trivalent cations. We acknowledge however that if Cr and Fe^{3+} are not considered, the absolute computed temperature might be slightly biased to lower values. The extent of the biasing is considered for the case of Cr. The Cr content from the samples used in the calibration is 0.21 (Bromiley and Pawley, 2003) and 0.34 apfu (Padrón-Navarta et al., 2010). This would increase the y_{atg} values by 0.025 and 0.043 (Table 2), respectively, which would result in a decrease of δH_{atgts} of ca. 0.5 kJ. Considering the scattering of the enthalpic correction, this effect can be ignored. Therefore, Cr contents of <0.1 apfu (the most common situation) would increase the temperature by ca. 10 °C, whereas for 0.04 apfu Cr, this increase would reach 20–30 °C. The effect of the ferric iron in the estimated temperature cannot be evaluated but we believe that it might affect the temperature calculation in the same direction. Therefore, a conservative uncertainty of 30–40 °C in the estimated temperature by using the proposed model seems reasonable.

5.3. Implications for water liberation in high grade serpentinites

The solution model for antigorite in the FMASH system does not change significantly the phase relations established in the simple CMSH system. Nevertheless, more information is gained on the PT conditions for the antigorite maximum thermal stability, which are in line with previous experiments. Antigorite from a serpentinite with a spinel harzburgite composition (e.g. Al06-44, Fig. 4) will be stable at up to ca. 670 °C at 20 kbar by using this model, which is 30 °C higher than in the FMSH system for the same sample. It is anticipated that Cr_2O_3 and Fe_2O_3 plays a similar role to that of Al_2O_3, i.e., that it increases the maximum temperature stability of antigorite. The higher stability of antigorite influences the position of water liberation in subduction zone models (e.g. Hacker et al., 2003). This will have an impact on the position of dehydration related earthquakes (Hacker et al., 2003) as well as on models for water fluxes as a function of depth in subduction zones (van Keken et al., 2011).

In an isobaric section at 30 kbar through the calculated phase diagram section presented earlier (Fig. 6), antigorite decomposition is the main water producing reaction (Fig. 7), but dehydration reactions involving brucite and chlorite are also significant. One consequence of having a more realistic thermodynamic solution model for antigorite is that the nature of the dehydration reaction changes. In the MSH system, the reaction of antigorite to olivine, orthopyroxene and fluid is univariant, and hence all the fluid is liberated in one single pulse. Instead, in the more complex FMASH system, the antigorite breakdown reaction occurs in a divariant field over a 20 °C interval. This is an important fact for experiments addressing the kinetics of the antigorite dehydration (e.g. Chollet et al., 2011; Eggler and Ehmann, 2010; Perrillat et al., 2005), because the assumption of a simplified univariant reaction is not justified in nature. A more accurate modeling of the antigorite dehydration reaction would be also useful to predict the rate of fluid production (e.g. Chollet et al., 2011; Eggler and Ehmann, 2010) with important implications for our understanding of fluid migration in subduction zones. During the breakdown of antigorite, the aluminum is incorporated into newly formed chlorite (reaction (3)). As a consequence the amount of water liberated is less than the total amount of water hosted in antigorite (Fig. 7). Indeed, in most of the antigorite dehydration kinetic experiments the occurrence of chlorite as a reaction products is not acknowledged and therefore such experiments overestimate the fluid production rates.

In the previous section, we have shown that the Al content in antigorite changes continuously when it is buffered with chlorite and olivine according to reaction (1). This reaction also liberates trivial amounts of fluid and hence prograde metamorphism through the Atg–Chl–Ol stability field (Fig. 4) is associated with a constant production of small amounts of fluid. Fig. 7 shows that about 0.1 wt.% of H_2O is liberated through this continuous reaction. These small amounts of fluids would enhance the transformation of the antigorite polysome with increasing temperature which, in turn, would trigger further release of fluid. Wunder et al. (2001) suggested that the antigorite polysome should change from 18 to 14 when temperature is increased from 450 °C to 650 °C at 30 kbar. The change in polysomatism would add 0.19 wt.% of H_2O (Wunder et al., 2001) to the 0.1 wt.% associated to the increase in Al-content in antigorite over ca. 100–150 °C. While such a small amount of fluid has only a marginal impact on the fluid budget in subducted serpentinites it can highly influence their rheology.

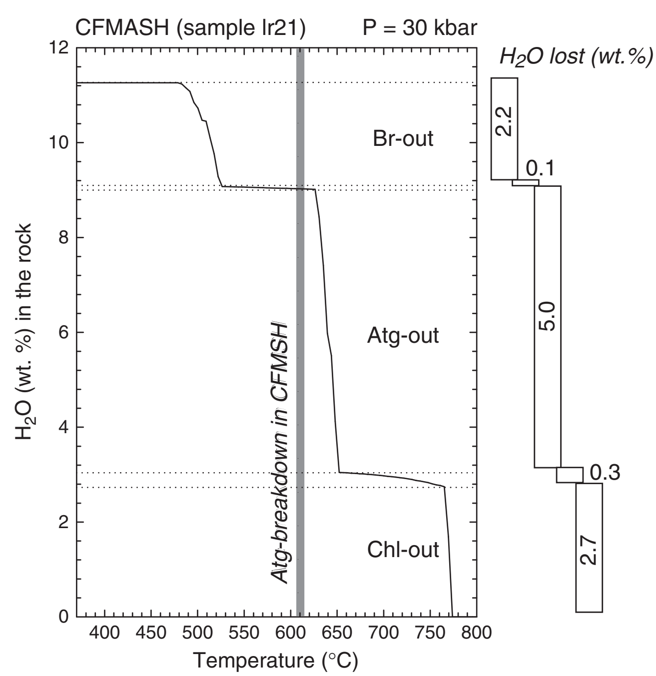

Fig. 7. Evolution of the water content in a serpentinized lherzolite (cf. Fig. 6) during heating at constant pressure (30 kbar). Sharp steps correspond with the dehydration of brucite, antigorite and chlorite. The gently step between brucite and antigorite dehydration is the results of the small release of fluid associated to the increase in Al-content with temperature in antigorite (reaction (1)). Numbers in the right boxes indicate the amount of water (in wt.%) liberated in each step.

The relative importance of dissolution–precipitation processes over dislocation creep as the dominant deformation mechanism for serpentinites is still a matter of debate (Reynard, 2013). Small but continuous release of fluid in the antigorite stability field during subduction might favor dissolution–precipitation processes over dislocation creep to accommodate strain resulting in a Newtonian rheology (Wassmann et al., 2011). On the contrary, fluid saturated condition will be less likely to occur during exhumation because of the low porosity of serpentinite and because reaction (1) is now consuming fluid with decreasing temperature. Under these conditions serpentinite will be stronger and deformation by dislocation creep (power law rheology) will be dominant (Padrón-Navarta et al., 2012).

6. Concluding remarks

An ideal solution model has been developed to account for the Al incorporation in antigorite through a Tschermak's substitution. The model has been calibrated against experimental works in the FMASH system and correctly predicts the Al-content observed in natural Atg–serpentinite and Ca-bearing serpentinite. The use of the Al-content in antigorite as a geothermometer is applicable to a wide range of ultramafic rock compositions. Most spinel harzburgites and all lherzolitic compositions will develop mineral assemblages in which the Al content of antigorite depends on pressure and temperature. Hence, the Tschermak's exchange in antigorite can be used to constrain metamorphic conditions in metamorphosed ultramafic rocks.

Although several assumptions were made on the formulation of the model and the problems detected in the modeling of Al-poor chlorite, this contribution represents a further step to explore the complex interrelation between the occurrence of minor components in antigorite and its modular structure (polysomatism). Moreover, the extension of the antigorite solution model to the CFMASH system gives us the opportunity to model more precisely the location of dehydration reactions and fluid rate production in subduction zones.

Acknowledgments

We thank B. Reynard for inviting us to send this contribution to the Lithos special volume on serpentinites. A. Pawley and G. Bromiley are deeply thanked for providing chemical data from their experiments. We gratefully acknowledge constructive reviews by C. Groppo, and an anonymous reviewer and comments by the editors of this volume. The research leading to these results has been partially funded by HISLa-DR, an EU FP7-funded Marie Curie Action under grant agreement PIOF-GA-2010-273017. VLSV's, MTGP's and CG's work were funded by the Spanish “Ministerio de Economía y Competitividad” (grants CGL2009-12518/BTE, CGL2010-14848/BTE and CGL2012-32067), “Junta de Andalucía” (research groups RNM-145, RNM-131 and grant 2009RNM-4495) and International Lithosphere Program (CC4-MEDYNA). CM's research has been supported by an EU-FP7-funded Marie Curie postdoctoral grant under contract agreement PERG08-GA-2010-276867.

References

Agard, P., Yamato, P., Jolivet, L., Burov, E., 2009. Exhumation of oceanic blueschists and eclogites in subduction zones: timing and mechanisms. Earth-Science Reviews 92, 53–79.
Albino, G.V., 1995. Iron-rich and aluminum-rich serpentine and chlorite from the boundary ultramafic complex, Cape-Smith Belt, New-Quebec. The Canadian Mineralogist 33, 559–568.
Angiboust, S., Wolf, S., Burov, E., Agard, P., Yamato, P., 2012. Effect of fluid circulation on subduction interface tectonic processes: insights from thermo-mechanical numerical modelling. Earth and Planetary Science Letters 357–358, 238–248.
Auzende, A.-L., Devouard, B., Guillot, S., Daniel, I., Baronnet, A., Lardeaux, J.-M., 2002. Serpentinites from Central Cuba: petrology and HRTEM study. European Journal of Mineralogy 14, 905–914.
Auzende, A.-L., Guillot, S., Devouard, B., Baronnet, A., 2006. Serpentinites in an Alpine convergent setting: effects of metamorphic grade and deformation on microstructures. European Journal of Mineralogy 18, 21–33.
Azer, M.K., Khalil, A.E.S., 2005. Petrological and mineralogical studies of Pan-African serpentinites at Bir Al-Edeid area, central Eastern Desert, Egypt. Journal of African Earth Sciences 43, 525–536.
Blais, J., Auvray, B., 1990. Serpentinization in the Archean komatiitic rocks of Kukmo greenstone belt, eastern Finland. The Canadian Mineralogist 28, 55–66.
Bowen, N.L., Tuttle, O.F., 1949. The system $MgO–SiO_2–H_2O$. Geological Society of America Bulletin 60, 439–460.
Bromiley, G.D., Pawley, A.R., 2003. The stability of antigorite in the systems $MgO–SiO_2–H_2O$ (MSH) and $MgO–Al_2O_3–SiO_2–H_2O$ (MASH): the effects of Al^{3+} substitution on high-pressure stability. American Mineralogist 88, 99–108.
Bucher-Nurminen, K., 1988. Compositional variation of phlogopite in a marble sample: implications for geological thermobarometry. Journal of Metamorphic Geology 6, 667–672.
Caruso, L.J., Chernosky, J.V., 1979. The stability of lizardite. The Canadian Mineralogist 17, 757–769.
Chernosky, J.V., Berman, R.G., Bryndzia, L.T., 1988. Stability, phase relations, and thermodynamic properties of chlorite and serpentinite group minerals. Reviews in Mineralogy and Geochemistry 19, 295–346.
Chollet, M., Daniel, I., Koga, K.T., Morard, G., Van de Moortèle, B., 2011. Kinetics and mechanism of antigorite dehydration: implications for subduction zone seismicity. Journal of Geophysical Research 116, B04203.
Connolly, J.A.D., 1990. Multivariable phase-diagrams — an algorithm based on generalized thermodynamics. American Journal of Science 290, 666–718.
Connolly, J.A.D., 2009. The geodynamic equation of state: what and how. Geochemistry, Geophysics, Geosystems 10.
Debret, B., Nicollet, C., Andreani, M., Schwartz, S., Godard, M., 2013. Three steps of serpentinization in an eclogitized oceanic serpentinization front (Lanzo Massif - Western Alps). Journal of Metamorphic Geology 31 (2), 165–186. http://dx.doi.org/10.1111/jmg.12008.
Dungan, M.A., 1977. Metastability in serpentine–olivine equilibria. American Mineralogist 62, 1018–1029.
Eggler, D.H., Ehmann, A.N., 2010. Rate of antigorite dehydration at 2 GPa applied to subduction zones. American Mineralogist 95, 761–769.
Evans, B.W., Johannes, W., Oterdoom, H., Trommsdorff, V., 1976. Stability of chrysotile and serpentinite in the serpentine multisystem. Schweizerische Mineralogische und Petrographische Mitteilungen 56, 79–93.
Evans, B.W., Dyar, M.D., Kuehner, S.M., 2012. Implications of ferrous and ferric iron in antigorite. American Mineralogist 97, 184–196.
Facer, J., Downes, H., Beard, A., 2009. In situ serpentinization and hydrous fluid metasomatism in spinel dunite xenoliths from the Bearpaw Mountains, Montana, USA. Journal of Petrology 50, 1443–1475.
Fockenberg, T., Schreyer, W., 1997. Synthesis and chemistry of unusual excess-Si aluminous enstatite in the system $MgO–Al_2O_3–SiO_2$ (MAS). European Journal of Mineralogy 9, 509–518.
Frost, R., 1975. Contact metamorphism of serpentinite, chloritic blackwall and rodingite at Paddy-Go-Easy Pass, Central Cascades, Washington. Journal of Petrology 16, 272–313.
Fuchs, Y., Linares, J., Mellini, M., 1998. Mossbauer and infrared spectrometry of lizardite-1T from Monte Fico, Elba. Physics and Chemistry of Minerals 26, 111–115.
Gerya, T.V., Stockhert, B., Perchuk, A.L., 2002. Exhumation of high-pressure metamorphic rocks in a subduction channel: a numerical simulation. Tectonics 21, 6–19.
Hacker, B.R., Abers, G.A., Peacock, S.M., 2003. Subduction factory — 1. Theoretical mineralogy, densities, seismic wave speeds, and H_2O contents. Journal of Geophysical Research — Solid Earth 108, 2029.
Hermann, J., Müntener, O., Scambelluri, M., 2000. The importance of serpentinite mylonites for subduction and exhumation of oceanic crust. Tectonophysics 327, 225–238.
Hilairet, N., Reynard, B., 2009. Stability and dynamics of serpentinite layer in subduction zone. Tectonophysics 465, 24–29.
Hilairet, N., Daniel, I., Reynard, B., 2006a. Equation of state of antigorite, stability field of serpentines, and seismicity in subduction zones. Geophysical Research Letters 33. http://dx.doi.org/10.1029/2005gl024728.
Hilairet, N., Daniel, I., Reynard, B., 2006b. P–V equations of state and the relative stabilities of serpentine varieties. Physics and Chemistry of Minerals 33, 629–637.
Holland, T., Powell, R., 1996. Thermodynamics of order–disorder in minerals 2. Symmetric formalism applied to solid solutions. American Mineralogist 81, 1425–1437.
Holland, T.J.B., Powell, R., 1998. An internally consistent thermodynamic data set for phases of petrological interest. Journal of Metamorphic Geology 16, 309–343.
Holland, T., Baker, J., Powell, R., 1998. Mixing properties and activity–composition relationships of chlorites in the system $MgO–FeO–Al_2O_3–SiO_2–H_2O$. European Journal of Mineralogy 10, 395–406.
Khalil, A.E.S., Azer, M.K., 2007. Supra-subduction affinity in the Neoproterozoic serpentinites in the Eastern Desert, Egypt: evidence from mineral composition. Journal of African Earth Sciences 49, 136–152.
Khedr, M.Z., Arai, S., 2010. Hydrous peridotites with Ti-rich chromian spinel as a low-temperature forearc mantle facies: evidence from the Happo-O'ne metaperidotites (Japan). Contributions to Mineralogy and Petrology 159, 137–157.
Khedr, M.Z., Arai, S., 2012. Petrology and geochemistry of prograde deserpentinized peridotites from Happo-O'ne, Japan: evidence of element mobility during deserpentinization. Journal of Asian Earth Sciences 225–241.
Khedr, M.Z., Arai, S., Tamura, A., Morishita, T., 2010. Clinopyroxenes in high-P metaperidotites from Happo-O'ne, central Japan: implications for wedge-transversal chemical change of slab-derived fluids. Lithos 119 (3–4), 439–456.
Li, X.P., Rahn, M., Bucher, K., 2004. Serpentinites of the Zermatt-Saas ophiolite complex and their texture evolution. Journal of Metamorphic Geology 22, 159–177.
López Sánchez-Vizcaíno, V., Trommsdorff, V., Gómez-Pugnaire, M.T., Garrido, C.J., Müntener, O., Connolly, J.A.D., 2005. Petrology of titanian clinohumite and olivine

at the high-pressure breakdown of antigorite serpentinite to chlorite harzburgite (Almirez Massif, S. Spain). Contributions to Mineralogy and Petrology 149, 627–646.
Malatesta, C., Crispini, L., Federico, L., Capponi, G., Scambelluri, M., 2012. The exhumation of high pressure ophiolites (Voltri Massif, Western Alps): insights from structural and petrologic data on metagabbro bodies. Tectonophysics 568-569, 102–123.
Mellini, M., Trommsdorff, V., Compagnoni, R., 1987. Antigorite polysomatism-behavior during progressive metamorphism. Contributions to Mineralogy and Petrology 97, 147–155.
Müntener, O., Hermann, J., 1994. Titanian andradite in a metapyroxenite layer from the Malenco ultramafics (Italy) — implications for Ti-mobility and low-oxygen fugacity. Contributions to Mineralogy and Petrology 116, 156–168.
Nestola, F., Angel, R., Zhao, J., Garrido, C., López Sánchez-Vizcaíno, V., Capitani, G., Mellini, M., 2010. Antigorite equation of state and anomalous softening at 6 GPa: an in situ single-crystal X-ray diffraction study. Contributions to Mineralogy and Petrology 160, 33–43.
Nozaka, T., 2005. Metamorphic history of serpentinite mylonites from the Happo ultramafic complex, central Japan. Journal of Metamorphic Geology 23, 711–723.
Nozaka, T., Ito, Y., 2011. Cleavable olivine in serpentinite mylonites from the Oeyama ophiolite. Journal of Mineralogical and Petrological Sciences 106, 36–50.
O'Hanley, D.S., 1996. Serpentinites: records of petrologic and tectonic history. Oxford Monographs on Geology and Geophysics, 34 (277 pp.).
O'Hanley, D.S., Wicks, F.J., 1995. Conditions of formation of lizardite, chrysotile and antigorite, Cassiar, British-Columbia. The Canadian Mineralogist 33, 753–773.
Padrón-Navarta, J.A., López Sánchez-Vizcaíno, V., Garrido, C.J., Gómez-Pugnaire, M.T., Jabaloy, A., Capitani, G., Mellini, M., 2008. Highly ordered antigorite from Cerro del Almirez HP–HT serpentinites, SE Spain. Contributions to Mineralogy and Petrology 156, 679–688.
Padrón-Navarta, J.A., Hermann, J., Garrido, C., López Sánchez-Vizcaíno, V., Gómez-Pugnaire, M.T., 2010. An experimental investigation of antigorite dehydration in natural silica-enriched serpentinite. Contributions to Mineralogy and Petrology 159, 25–42.
Padrón-Navarta, J.A., López Sánchez-Vizcaíno, V., Garrido, C.J., Gómez-Pugnaire, M.T., 2011. Metamorphic record of high-pressure dehydration of antigorite serpentinite to chlorite harzburgite in a subduction setting (Cerro del Almirez, Nevado–Filábride Complex, Southern Spain). Journal of Petrology 52, 2047–2078.
Padrón-Navarta, J.A., Tommasi, A., Garrido, C.J., López Sánchez-Vizcaíno, V., 2012. Plastic deformation and development of antigorite crystal preferred orientation in high-pressure serpentinites. Earth and Planetary Science Letters 349–350, 75–86.
Peretti, A., Dubessy, J., Mullis, J., Frost, B.R., Trommsdorff, V., 1992. Highly reducing conditions during Alpine metamorphism of the Malenco peridotite (Sondrio, northern Italy) indicated by mineral paragenesis and H_2 in fluid inclusions. Contributions to Mineralogy and Petrology 112, 329–340.
Perrillat, J.P., Daniel, I., Koga, K.T., Reynard, B., Cardon, H., Crichton, W.A., 2005. Kinetics of antigorite dehydration: a real-time X-ray diffraction study. Earth and Planetary Science Letters 236, 899–913.
Proenza, J.A., Ortega-Gutiérrez, F., Camprubí, A., Tritlla, J., Elías-Herrera, M., Reyes-Salas, M., 2004. Paleozoic serpentinite-enclosed chromitites from Tehuitzingo (Acatlán Complex, southern Mexico): a petrological and mineralogical study. Journal of South American Earth Sciences 16, 649–666.
Rebay, G., Spalla, M.I., Zanoni, D., 2012. Interaction of deformation and metamorphism during subduction and exhumation of hydrated oceanic mantle: insights from the Western Alps. Journal of Metamorphic Geology 30, 687–702.
Reynard, B., 2013. Serpentine in active subduction zones. Lithos 178, 171–185.
Torres-Roldán, R.L., García-Casco, A., García-Sanchez, P.A., 2000. CSpace: an integrated workplace for the graphical and algebraic analysis of phase assemblages on 32-bit wintel platforms. Computers & Geosciences 26 (7), 779–793.
Rüpke, L.H., Phipps Morgan, J., Hort, M., Connolly, J.A.D., 2004. Serpentine and the subduction zone water cycle. Earth and Planetary Science Letters 223, 17–34.
Scambelluri, M., Hoogerduijn Strating, E.H., Piccardo, G.B., Vissers, R.L.M., Rampone, E., 1991. Alpine olivine- and titanian clinohumite-bearing assemblages in the Erro-Tobbio peridotite (Voltri Massif, NW Italy). Journal of Metamorphic Geology 9, 79–91.
Scambelluri, M., Muntener, O., Hermann, J., Piccardo, G.B., Trommsdorff, V., 1995. Subduction of water into the mantle — history of an alpine peridotite. Geology 23, 459–462.
Schmidt, M.W., Poli, S., 1998. Experimentally based water budgets for dehydrating slabs and consequences for arc magma generation. Earth and Planetary Science Letters 163, 361–379.
Schwartz, S., Guillot, S., Reynard, B., Lafay, R., Debret, B., Nicollet, C., Lanari, P., Auzende, A.L., 2013. Pressure–temperature estimates of the lizardite/antigorite transition in high pressure serpentinites. Lithos 178, 197–210.
Smith, D., 2010. Antigorite peridotite, metaserpentinite, and other inclusions within diatremes on the Colorado Plateau, SW USA: implications for the mantle wedge during low-angle subduction. Journal of Petrology 51, 1355–1379.
Tajčmanová, L., Connolly, J.A.D., Cesare, B., 2009. A thermodynamic model for titanium and ferric iron solution in biotite. Journal of Metamorphic Geology 27, 153–165.
Trommsdorff, V., Connolly, J.A.D., 1996. The ultramafic contact aureole about the Bregaglia (Bergell) tonalite: isograds and a thermal model. Schweizerische Mineralogische und Petrographische Mitteilungen 76, 537–547.
Trommsdorff, V., Evans, B.W., 1972. Progressive metamorphism of antigorite schist in the Bergell tonalite aureole (Italy). American Journal of Science 272, 423–437.
Trommsdorff, V., Evans, B.W., 1974. Alpine metamorphism of peridotitic rocks. Schweizerische Mineralogische und Petrographische Mitteilungen 72, 229–242.
Trommsdorff, V., López Sánchez-Vizcaíno, V., Gómez-Pugnaire, M.T., Müntener, O., 1998. High pressure breakdown of antigorite to spinifex-textured olivine and orthopyroxene, SE Spain. Contributions to Mineralogy and Petrology 132, 139–148.
Uehara, S., Kamata, K., 1994. Antigorite with a large supercell from Saganoseki, Oita Prefecture, Japan. The Canadian Mineralogist 32, 93–103.
Uehara, S., Shirozu, H., 1985. Variations in chemical composition and structural properties of antigorites. Mineralogical Journal 12, 299–318.
Ulmer, P., Trommsdorff, V., 1995. Serpentine stability to mantle depths and subduction-related magmatism. Science 268, 858–861.
Ulmer, P., Trommsdorff, V., 1999. Phase relations of hydrous mantle subducting to 300 km. In: Fei, Y., Bertka, C.M., Mysen, B.O. (Eds.), Mantle Petrology: Field observations and High Pressure Experimentation. The Geochemical Society, pp. 259–281.
Van Keken, P.E., Hacker, B.R., Syracuse, E.M., Abers, G.A., 2011. Subduction factory: 4. Depth-dependent flux of H_2O from subducting slabs worldwide. Journal of Geophysical Research 116, B01401.
Vance, J.A., Dungan, M.A., 1977. Formation of peridotites by deserpentinization in the Darrington and Sultan areas, Cascade Mountains, Washington. Geological Society of America Bulletin 88, 1497–1508.
Viti, C., Mellini, M., 1997. Contrasting chemical compositions in associated lizardite and chrysotile in veins from Elba, Italy. European Journal of Mineralogy 9, 585–596.
Wassmann, S., Stöckhert, B., Trepmann, C.A., 2011. Dissolution precipitation creep versus crystalline plasticity in high-pressure metamorphic serpentinites. Geological Society, London, Special Publications 360, 129–149.
Wei, C., Powell, R., 2003. Phase relations in high-pressure metapelites in the system KFMASH (K_2O–FeO–MgO–Al_2O_3–SiO_2–H_2O) with application to natural rocks. Contributions to Mineralogy and Petrology 145, 301–315.
White, R.W., Powell, R., Phillips, G.N., 2003. A mineral equilibria study of the hydrothermal alteration in mafic greenschist facies rocks at Kalgoorlie, Western Australia. Journal of Metamorphic Geology 21, 455–468.
Whitney, D.L., Evans, B.W., 2010. Abbreviations for names of rock-forming minerals. American Mineralogist 95, 185–187.
Wicks, F.J., O'Hanley, D.S., 1988. Serpentine minerals: structure and petrology. Reviews in Mineralogy 19, 91–167.
Wicks, F.J., Plant, A.G., 1979. Electron-microprobe and X-ray microbeam studies of serpentine textures. The Canadian Mineralogist 17, 785–830.
Worden, R.H., Droop, G.T.R., Champness, P.E., 1991. The reaction antigorite = olivine + talc + H_2O in the Bergell aureole, N. Italy. Mineralogical Magazine 55, 367–377.
Wunder, B., 1998. Equilibrium experiments in the system MgO–SiO_2–H_2O (MSH): stability fields of clinohumite–OH ($Mg_9Si_4O_{16}(OH)_2$), chondrodite–OH ($Mg_5Si_2O_8(OH)_2$) and phase A ($Mg_7Si_2O_8(OH)_6$). Contributions to Mineralogy and Petrology 132, 111–120.
Wunder, B., Schreyer, W., 1997. Antigorite: high-pressure stability in the system MgO–SiO_2–H_2O (MSH). Lithos 41, 213–227.
Wunder, B., Wirth, R., Gottschalk, M., 2001. Antigorite: pressure and temperature dependence of polysomatism and water content. European Journal of Mineralogy 13, 485–495.
Yang, J.-J., Powell, R., 2008. Ultrahigh-pressure garnet peridotites from the devolatilization of sea-floor hydrated ultramafic rocks. Journal of Metamorphic Geology 26, 695–716.